Geomechanics and Engineering, *Vol. 25, No. 6 (2021) 455-471*
DOI: https://doi.org/10.12989/gae.2021.25.6.455

Interaction between rock bolt and rock bridge under tensile loading

Vahab Sarfarazi*[1], Kaveh Asgari[2a] and Mehdi Nasrollahi[3b]

[1]*Department of Mining Engineering, Hamedan University of Technology, Hamedan, Iran*
[2]*Department of Mining Engineering, Shahid Bahonar University of Kerman, Kerman, Iran*
[3]*Department of Civil Engineering, Azad University of Hamedan, Hamedan, Iran*

(Received January 5, 2021, Revised June 5, 2021, Accepted June 11, 2021)

Abstract. The objective of this study is investigating the effect of loading rates on the interaction between rock bolts and rock bridges using experimental test and numerical simulation. A new test set up was developed experimentally for determination of tensile strength of bridge area. A concrete block with dimensions of 15 × 15 × 10 cm consisting non-persistent notch was prepared and subjected to tensile loading using special loading set up. The configuration of non-persistent joint was different in various samples. A 30-ton hydraulic load cell applied tensile loading to concrete complex with a high-pressure rate of 0.01 mm per second. Simultaneously with experimental test, numerical simulation was performed on the tensile behavior of non-persistent joint adjacent to rock bolt. Two sets of non-persistent joint were prepared. The first sets were similar to experimental one while, in the second sets, two edge joints with lengths of 1.5 cm, 3 cm and 4.5 cm were prepared. The angle of these joint related to horizontal axis were 0, 15, 30, 45, 60, 75, and 90. Also, the rock bolts adjacent to joints were simulated and were subjected to tensile loading with two high and low loading rates i.e. 0.01 mm/sec and 0.0001 mm/sec. The results showed that the crack propagation angle related to tensile load direction was decreased by decreasing the tensile loading rate. The tensile failure stress decreased by presence of pre-existing crack within the model. Tensile failure stress had minimum value whenever the angle of pre-existing crack was 0°. The numerical results were in a good accordance with experimental ones.

Keywords: tensile strength; rock bolt; tensile crack; PFC2D

1. Introduction

Jointed rock masses are common in many underground excavation projects. Other challenges include shallow ground level construction, which can cause a variety of problems such as face failure, lengthening in progress, and harm to surface constructions (Das *et al.* 2017; Dias, 2011). For the reasons mentioned, in underground constructions, special attention should be paid to the stability of the work face and the necessary precautions of a suitable support system. In addition, possible ground movements in the direction of tunneling must be binned because, underground excavations change the intensity and the direction of stresses, the extent of these changes depends mainly on the pre-excavated in situ stress and form of excavation. These distributed stresses form a turbulent area of failed rock blocks around the drilling boundary. In some cases, the magnitude of in-situ stresses in competent rocks is low, in these kinds of situations the rock mass can act like an elastic component and the disordered zone may not be formed (Goel *et al.* 2007). Several factors affect the stability of tunnels including, rock mass characterization, in situ stresses, geological situation, blasting-induced dynamic loading, and support systems. Bolts limit deformation in the rock mass and thus strengthen it. Shear loads are generally transmitted from bolts to the host rock mass. Characteristics of the cement grout compound determine some factors such as, the nature of load transfer, bolting system type and quality of the rock adjacent to the bolt. Thus, to ameliorate the design of bolting, it's vital to have a great comprehension of the behavior of rock bolts in deformed jointed rock masses. two main components of the rock mass, which include the distinct intact rock Characteristics and rock joint Characteristics, determine the total response of the rock mass (Singh *et al.* 2002). Rock joints induce impotence and deformability to the rock masses; hence, they have a significant effect on the deformational behavior of a rock mass. The area between two neighboring joints was called rock bridge. The terms joint normal stiffness (K_n) and shear stiffness (K_s) are used in rock engineering to quantify the joint strength. Barton (1986) inclined that, these two factors are primarily relying on stress and may applying tension can eliminate them. Understanding the phenomenon of complex deformation of rock mass depends on separation the unique ingredients of deformation, include, (1) intact rock (elastic or pseudo-elastic) ingredient separated by the joints, (2) joint normal stress component, and (3) joint shear stress component. But in jointed rock blocks the failure phenomena are much more complex and it and involves a set of several failure mechanisms .In most cases, several discontinuities are seen in each rock (weakest planes in the rock mass). These primary properties play a

∗Corresponding author, Ph.D.
E-mail: Sarfarazi@hut.ac.ir
[a]Research Scholar
E-mail: kavehaskary1373@gmail.com
[b]Research Scholar
E-mail: nasrollahi_mehdi@yahoo.com

ISSN: 2005-307X (Print), 2092-6219 (Online)

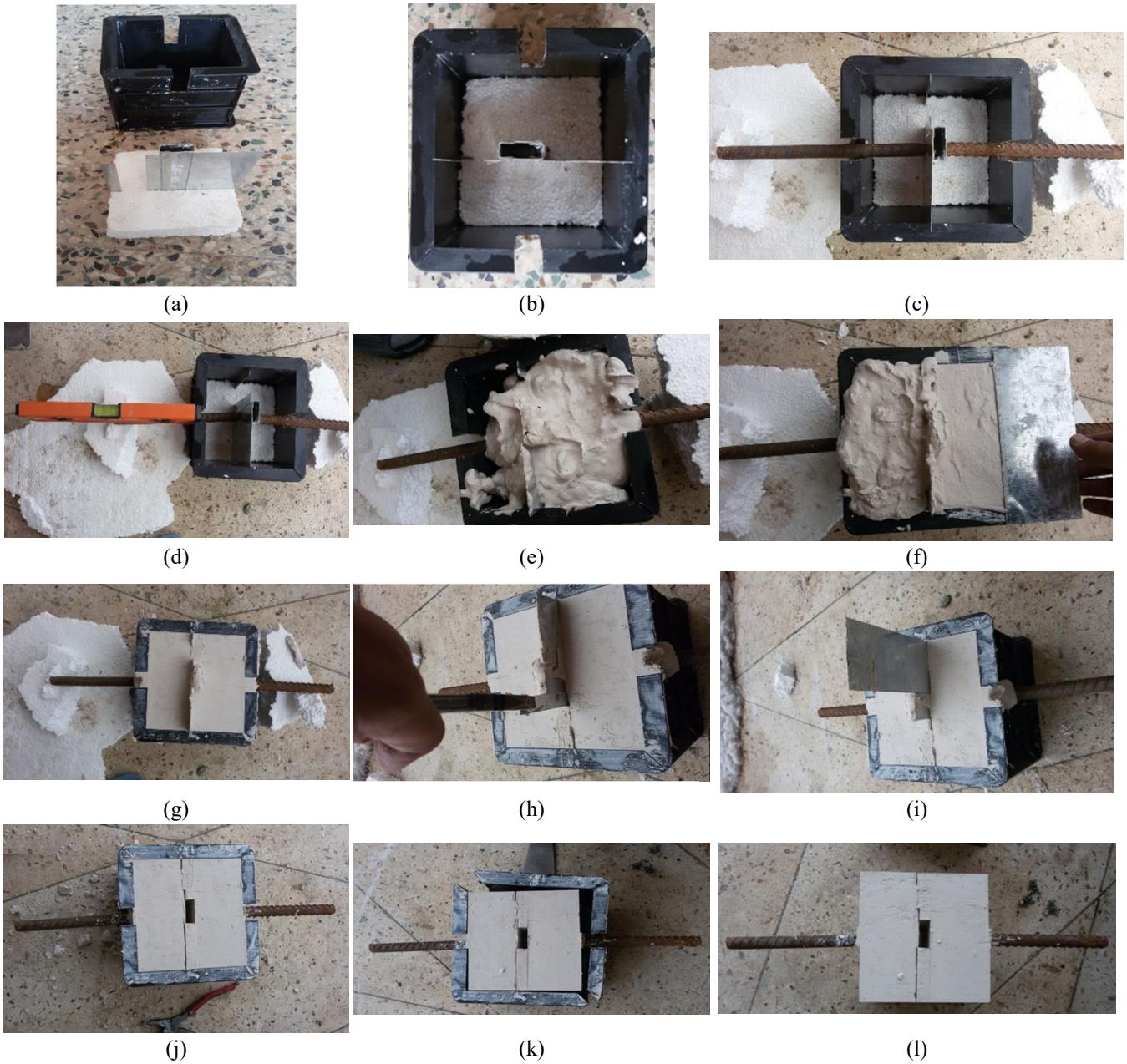

Fig. 1 (a) box model, (b) The plates within the model, c) The anchor within the mold, (d) Leveling the anchor, (e) Mixture into the mold, (f) Flatting the upper surface, (g) Removing the plates, (h) Removing the plates,(i) model with preexisting notch inside the mold, (j) Opening the mold and (k) model with preexisting notch

great role in forming a damage zone (Singh and Xavier 2005). As reported by Ramulu *et al.* (2009) ‘‘over break zone” rock blocks totally separate from the rock mass and this area exceeds the minimum quarry line of the determined boundary. While, the ‘‘damage zone” initiates from the outer edge of the over break area (Saiang and Nordlund (2009). Usually due to mining activates such as drilling and blasting, a lattice of micro cracks and fractures formed and these fractures lead to irretrievable changes in rock mass properties. Eventually, the ‘‘disturbed zone” spreads just from the damage zone boundary. In this zone, the difference in the rock mass characteristics are reversible, and just predominant changes are related to the hydraulic permeability and stress (Palmstro¨m and Singh 2001, Shen and Barton 1997, Lin *et al.* 2020a, b). Different parameters such as construction cost, Prolongation and tunnel stability significantly depend on the over break zone and the damage zone. Rock bolt supports are the best and economical ways for controlling rock mass accidents in underground constructions (Li *et al.* 2015, 2017, Wang *et al.* 2018, Zou 2016, Zhao 2018, Kim 2018, Wang 2019, Lin *et al.* 2020c, Cao *et al.* 2020, Hu *et al.* 2020, Luo *et al.* 2020). Rock bolt is usually emplaced in the jointed and fractured rock mass and based on the relative location of the bolt and the loading direction is subject to the accumulation of bending, axial, and shear loads. In addition, the overall strength of a jointed rock mass can be improved by the installing rock bolts (Forbes *et al.* 2017). In the previous research, there is

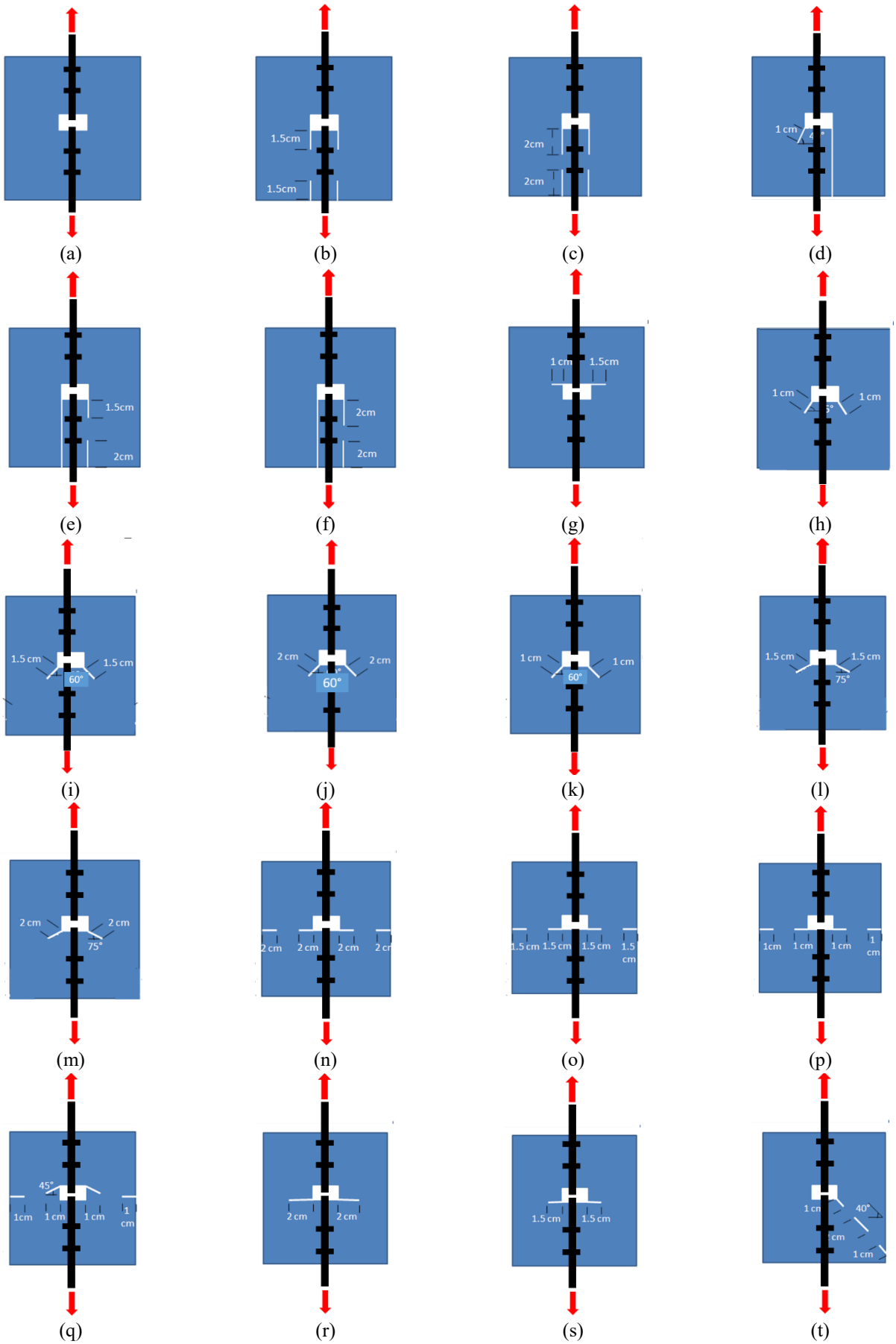

Fig. 2 The schematic view of samples consisting non-persistent joint

(u) (v)

Fig. 2 Continued

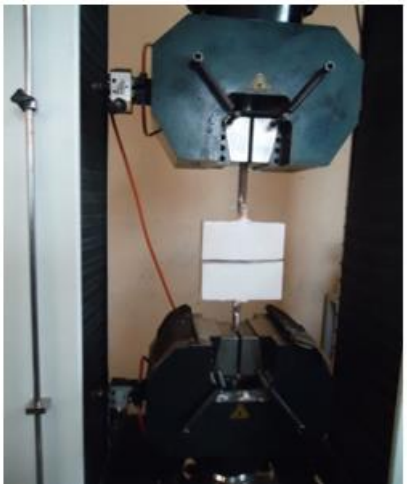

Fig. 3 The model with pre-existing notch in tensile device

not any study on the failure behavior of non-persistent joint adjacent to rock bolts. The aim of this paper is to study the interaction between the rock bolts and rock bridges using experimental test and numerical simulation.

2. Experimental studies

A series of laboratory tests were conducted to assess the performance of tensile device for determining the direct tensile strength of non-persistent crack.

2.1 Test material and preparation technique of the specimens

Firstly, a mold with dimensions s of 15 × 15 × 15 cm was fixed through screwing (Fig. 1(a)). Secondly, a plastic box with dimensions s of 15 × 15 × 5 cm was inserted at the end of the mold (Fig. 1(b)). This box was served as fixing the plate. The plate was inserted through the box (Fig. 1(b)). Dimensions of plates was 12 cm*1 mm. the wide of plates was different based on the wide of the joint. A central thicken sheet was sited in middle of the box (Fig. 1(b) and 1(c)). This sheet creates a hollow rectangular space in middle of the mold. In the final step two anchor bolt with diameter of 2cm and length of 40 cm go through the box via two notches which situated at the edges of the box (Fig. 1(c)). These anchors are leveled by special device (Fig. 1(d)). The concrete specimens were prepared from a mixture of two parts water, two parts cement and one part sand. The specimens were prepared by pouring slurry material in the containers (Figs. 1(e), 1(f) and 1(g)) and then leave it to hardened at room temperature for 8 hours. After the blocks were hardened, the plates were removed from the sample (Fig 1 h, i and j). The sample remained intact after removing the plates (Figs 1k and l). Fig 2 shows the schematic view of different samples with and without presence of notches. the anchor was fixed in the tensile test device and tensile loading was applied to samples at a rate of 0.01 mm/sec (Fig. 2)

3. Experimental results

3.1 Failure pattern of the experimental samples

a) The intact specimen without pre-existing notch

In this configuration, two cracks initiate from edge of rectangular space and scattered perpendicular to loading direction till coalescence with sample edge (Fig. 4(a)).

b) When notch angle is 90° and its lengths is 1.5 c*m:*

In this configuration two cracks initiates from upper notches and scattered perpendicular to the loading direction

Fig. 4 (a) failure pattern of intact model, (b) failure pattern of model consisting two vertical non persistent notch, (c) failure pattern of model consisting two vertical non persistent notch, (d) failure pattern of model consisting one oriented edge notch with angle of 40 and one persistent notch, (e) failure pattern of model consisting one vertical non persistent notch and one persistent notch; (f) failure pattern of model consisting one vertical non persistent notch and one persistent notch,(g) failure pattern of model consisting two edge notch; h) failure pattern of model consisting two oriented notch; (i) failure pattern of model consisting two oriented notch, (j) failure pattern of model consisting two oriented notch, (k) failure pattern of model consisting two oriented notch, (l) failure pattern of model consisting two oriented notch, (m) failure pattern of model consisting two oriented notch, (n) failure pattern of model consisting two horizontal non-persistent joint; (o) failure pattern of model consisting two horizontal non-persistent joint, (p) failure pattern of model consisting two horizontal non-persistent joint, (q) failure pattern of model consisting two oriented joints and two horizontal notch, (r) failure pattern of model consisting two horizontal edge notch, (s) failure pattern of model consisting two horizontal edge notch, (t) failure pattern of model consisting three oriented joint, (u) failure pattern of model consisting three oriented joint and (v) failure pattern of model consisting three oriented joint

(m)

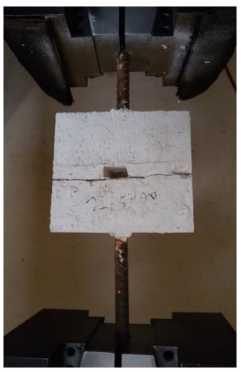

(n)

(o)

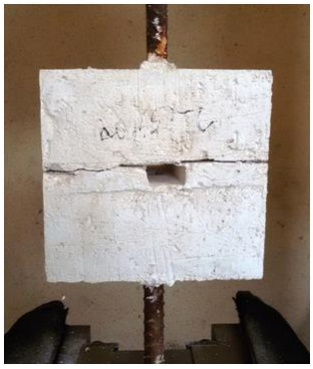

(p)

(q)

(r)

(s)

(t)

(u)

(v)

Fig. 4 Continued

till coalesces with model edge (Fig. 4(b)).

c)When notch angle is 90° and its lengths is 2 cm:

In this configuration two cracks initiates from upper notches and scattered perpendicular to the loading direction till coalesces with model edge (Fig. 4(c)).

d)The right notch angle is 90° and its length is 6.5 cm while the left notch angle is 40 and its length is 1 cm:

In this configuration one crack initiates from oriented notches and scattered perpendicular to the loading direction till coalesces with model edge (Fig. 4(d)).

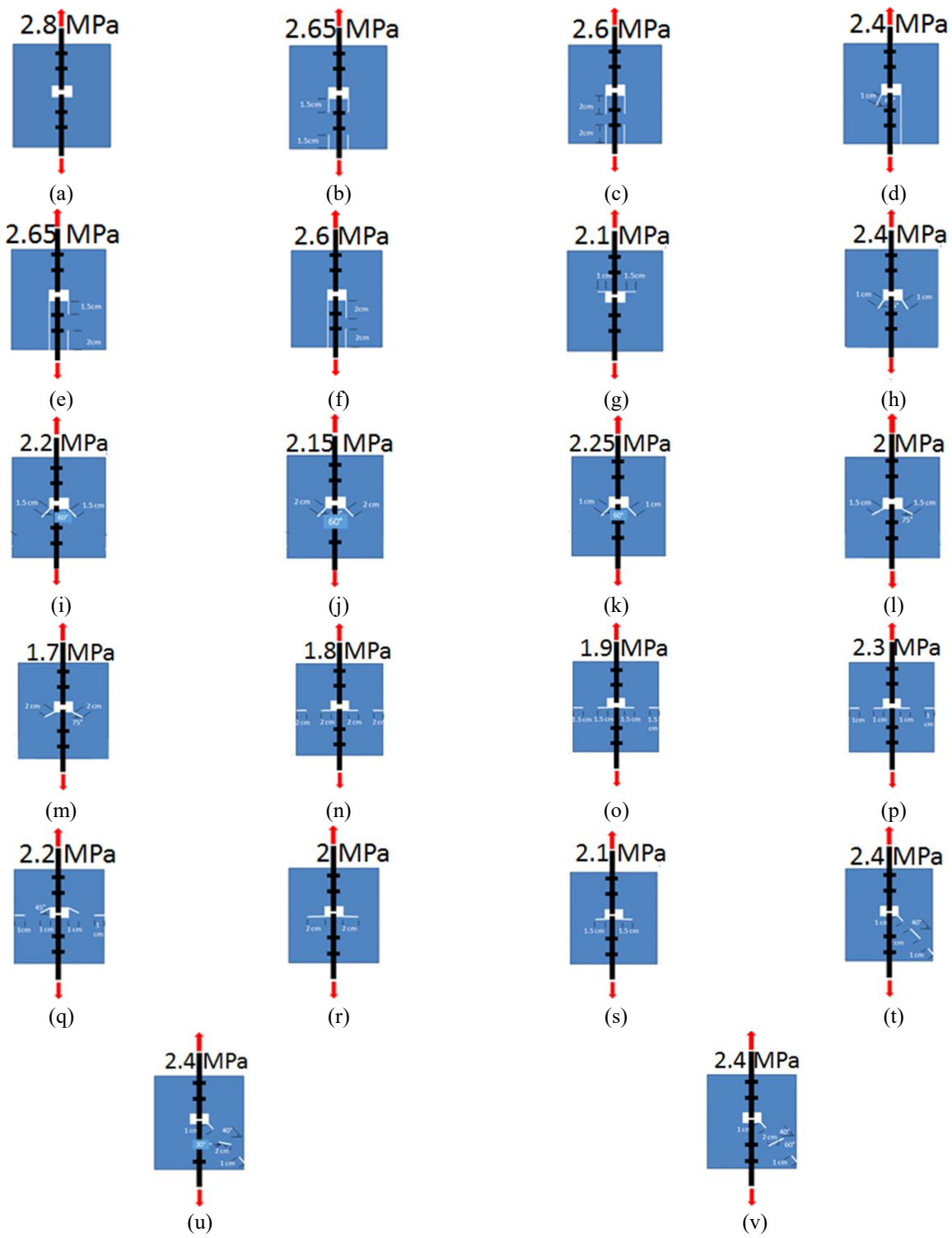

Fig. 5 The effect of specimen shape on the tensile failure force

e) The right non persistent notch angle is 90° and its lengths are 1.5 cm and 2 cm while the left persistent notch angle is 90 and its length is 6.5 cm:

In this configuration one crack initiates from non-persistent notches and scattered perpendicular to the loading direction till coalesces with model edge (Fig. 4(e)).

f) The right non persistent notch angle is 90° and its lengths are 2 cm and 2cm while the left persistent notch angle is 90 and its length is 6.5 cm:

In this configuration one crack initiates from non-persistent notches and scattered perpendicular to the loading direction till coalesces with model edge (Fig. 4(f)).

g) The right notch angle is 0° and its lengths is 1.5 cm while the left notch angle is 0 and its length is 1 cm:

In this configuration two cracks initiates from notches and scattered perpendicular to the loading direction till coalesces with model edge (Fig. 4(g)).

h) The non-persistent notches angles are 40° and its lengths are 1 cm:

In this configuration two cracks initiates from upper notches and scattered perpendicular to the loading direction till coalesces with model edge (Fig. 4(h)).

i)The non-persistent notch angles are 60° and its lengths are 1.5 cm:

In this configuration two cracks initiates from upper notches and scattered perpendicular to the loading direction till coalesces with model edge (Fig. 4(i)).

j) The non-persistent notches angles are 60° and its lengths are 2 cm:

In this configuration two cracks initiates from upper notches and scattered perpendicular to the loading direction till coalesces with model edge (Fig. 4(j)).

k) The notches angles are 60° and its lengths are 1 cm:

In this configuration two cracks initiates from upper notches and scattered perpendicular to the loading direction till coalesces with model edge (Fig. 4(k)).

l) The notches angles are 75° and its lengths are 1.5 cm:

In this configuration two cracks initiates from upper notches and scattered perpendicular to the loading direction till coalesces with model edge (Fig. 4(l)).

m) The notches angles are 75° and its lengths are 1 cm:

In this configuration two cracks initiates from upper notches and scattered perpendicular to the loading direction till coalesces with model edge (Fig. 4(m)).

n) The non-persistent notch angles are 0° and its lengths are 2 cm:

In this configuration two cracks initiates from internal notches and scattered perpendicular to the loading direction till coalesces with neighboring notches (Fig. 4(n)).

o) The non-persistent notch angle is 0° and its lengths are 1.5 cm:

In this configuration two cracks initiates from internal notches and scattered perpendicular to the loading direction till coalesces with neighboring notches (Fig. 4(o)).

p) The non-persistent notches angles are 0° and its lengths are 1 cm:

In this configuration two cracks initiates from internal notches and scattered perpendicular to the loading direction till coalesces with neighboring notches (Fig. 4(p)).

q) The edge notch angle is 45° and its lengths is 1 cm while other edge notch angle is 0° and its length is 1 cm:

In this configuration two cracks initiates from internal notches and scattered perpendicular to the loading direction till coalesces with neighboring notches (Fig. 4(q)).

r) The non-persistent notches angles are 0° and its lengths are 2 cm:

In this configuration two cracks initiates from notches and scattered perpendicular to the loading direction till coalesces with sample edge (Fig. 4(r))

s) The non-persistent notch angle is 0° and its lengths are 1.5 cm:

In this configuration two cracks initiates from notches and scattered perpendicular to the loading direction till coalesces with sample edge (Fig. 4(s)).

t) The right non-persistent notches angles are 40°; the length of upper and lower notch is 1 cm and the length of middle notch is 2 cm:

In this configuration tensile crack initiates from upper notch and scattered perpendicular to the loading direction till coalesces with sample edge. Another tensile crack initiates from rectangular shape space and scattered diagonally till coalesces with sample edge (Fig. 4(t)).

u) The right non-persistent notch angle is 40°; the length of upper and lower notch is 1 cm and the angle of middle notch related to joint surface was 30 and its length is 2 cm:

In this configuration tensile crack initiates from upper notch and scattered perpendicular to the loading direction till coalesces with sample edge. Another tensile crack initiates from rectangular shape space and scattered diagonally till coalesces with sample edge (Fig. 4(u)).

v)The right non-persistent notch angle is 40°; the length of upper and lower notch is 1 cm and the angle of middle notch related to joint surface was 60 and its length is 2 cm:

In this configuration tensile crack initiates from upper notch and scattered perpendicular to the loading direction till coalesces with sample edge. Another tensile crack initiates from rectangular shape space and scattered diagonally till coalesces with sample edge (Fig. 4(v)).

3.2 The effect of crack configuration on the tensile failure stress

Fig. 5 shows the effect of crack configuration on the tensile failure stress. Also, the failure stress in intact specimen has been depicted in this figure. Totally the following results could be rendered from Fig. 5.

- The tensile failure stress decreases by presence of pre-existing crack within the model.
- Tensile failure force has minimum value whenever the angle of pre-existing crack is 0°.
- The smaller the pre-existing crack length, the smaller the tensile failure stress.
- The angle of oriented middle pre-existing notch has not any effect on the tensile failure stress.
- The tensile failure stress is decreased by increasing the number of horizontal preexisting notches.

4. Numerical simulation

4.1 PFC2D and model generation

PFC2D usually uses for numerical simulations, for defining rock materials a compound of rigid circular disks connected at their points of contact. PFC is divided into contact-bond model and a parallel-bond model depending on its bonding models. The size range of parallel bond model is limited and acts between particles on a circular or rectangular cross section, while, the contact-bond because of its scarcely small size, acts only at the contact point, which can be represented by a the parallel-bond with zero radius. Based on the descriptions mentioned the contact-bond can only tolerate the force acting at the contact, while the parallel-bond can tolerate both the force and torque. There are five parameters that can active the parallel bonds, including normal and shear bond strength, normal and shear bond stiffness, and the bond radius, although, the bond stiffness and bond radius are not assigned in the contact-

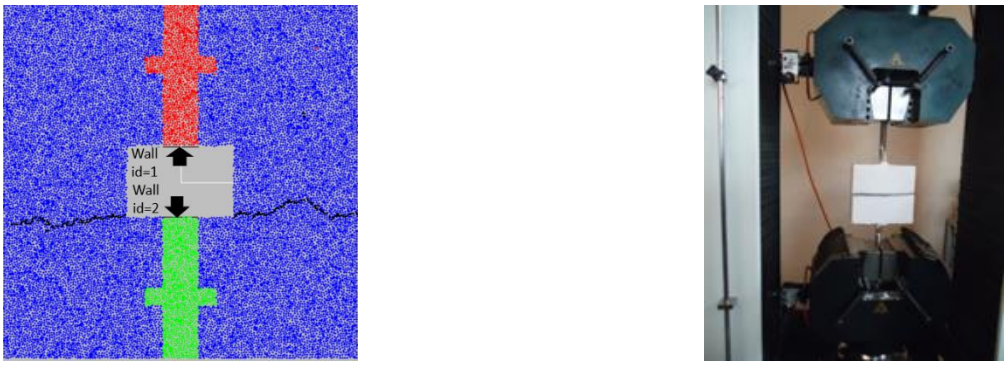

(a) (b)

Fig. 6 failure pattern of samples under (a) numerical tensile loading and (b) experimental tensile loading

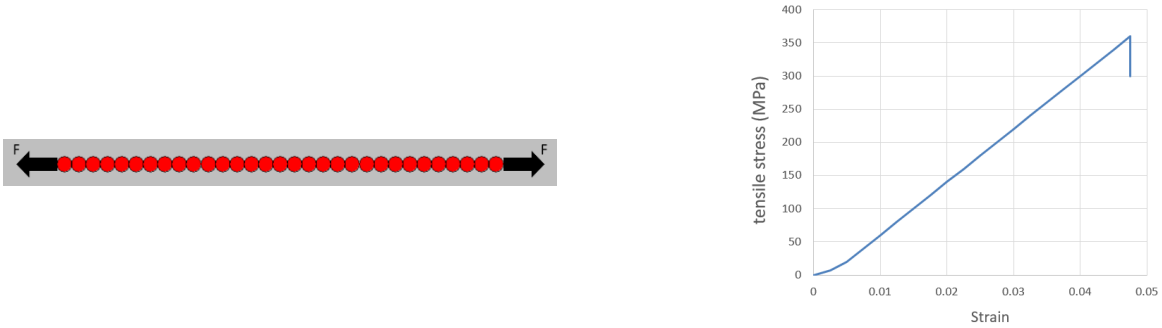

(a) (b)

Fig. 7 (a) rock bolt under tensile load and (b) tensile stress versus strain for rock bolt

Table 1 Micro parameter of rock bolt

Micro parameters	Value	Micro parameters	Value
disc radius (mm)	1	Parallel bond normal strength (MPa)	350±20
Disc density (kg.m^{-3})	7500	Parallel bond shear strength (MPa)	250±20
Disc contact modulus (GPa)	35	Parallel bond stiffness ratio	2.5
Disc stiffness ratio	1.3	Parallel bond radius multiplier	1
Disc friction coefficient	7	Parallel modulus (GPa)	35

Table 2 Comparison of macro-mechanical properties between experiments and model

Mechanical properties	Experimental results	PFC2D Model results
tensile strength (MPa)	3	3.1

Table 3 Micro properties used to represent the intact rock

Parameter	Value	Parameter	Value
Type of particle	Disc	Parallel-bond radius multiplier	1
Density	3000	Young's modulus of parallel bond (GPa)	9
Minimum radius	0.27	Parallel bond stiffness ratio	1.7
Size ratio	1.56	Particle friction coefficient	0.4
Porosity ratio	0.08	Parallel bond normal strength, mean (MPa)	10
Damping coefficient	0.7	Parallel bond normal strength, SD (MPa)	2.5
Contact Young's modulus	9	Parallel bond shear strength, mean (MPa)	40
Stiffness ratio	1.7	Parallel bond shear strength, SD (MPa)	10

bond model. If the applied stresses exceed the bond strengths, the both contact and parallel bonds will break (Itasca 2002, Potyondy and Cundall 2004). Bond breakage has different effect on these two models, In the contact-bond model, bond breakage does not have significant effect on the macro stiffness which causing the particles remain in contact. Since the stiffness is depending on contact stiffness and bond stiffness, in the parallel-bond model, bond breakage causes an immediate reduction in macro stiffness. Furthermore, with an associated decrease in stiffness the bonds may break in either tension or shearing, the parallel bond model can be more realistic for rock-like material modeling. Therefore, in this study, the parallel-bond model was selected. Before a parallel-bond model can be produced several micro parameters should be determined. These parameters including those that make the assembly consists of the varied sized circular disks reproduce the macro characteristics of the real material under uniaxial compression such as Young's modulus, UCS, and Poisson's ratio. To meet the real physical results and improving accuracy A calibration process is needed, which is attained by a "trial and error" process although several quantitative methods were proposed with the design of experiment and optimization method etc.

4.2 Preparation and calibration of the PFC2D model for rock-like material

In this paper for preparation a test model, the standard process of generating a PFC2D assembly were used

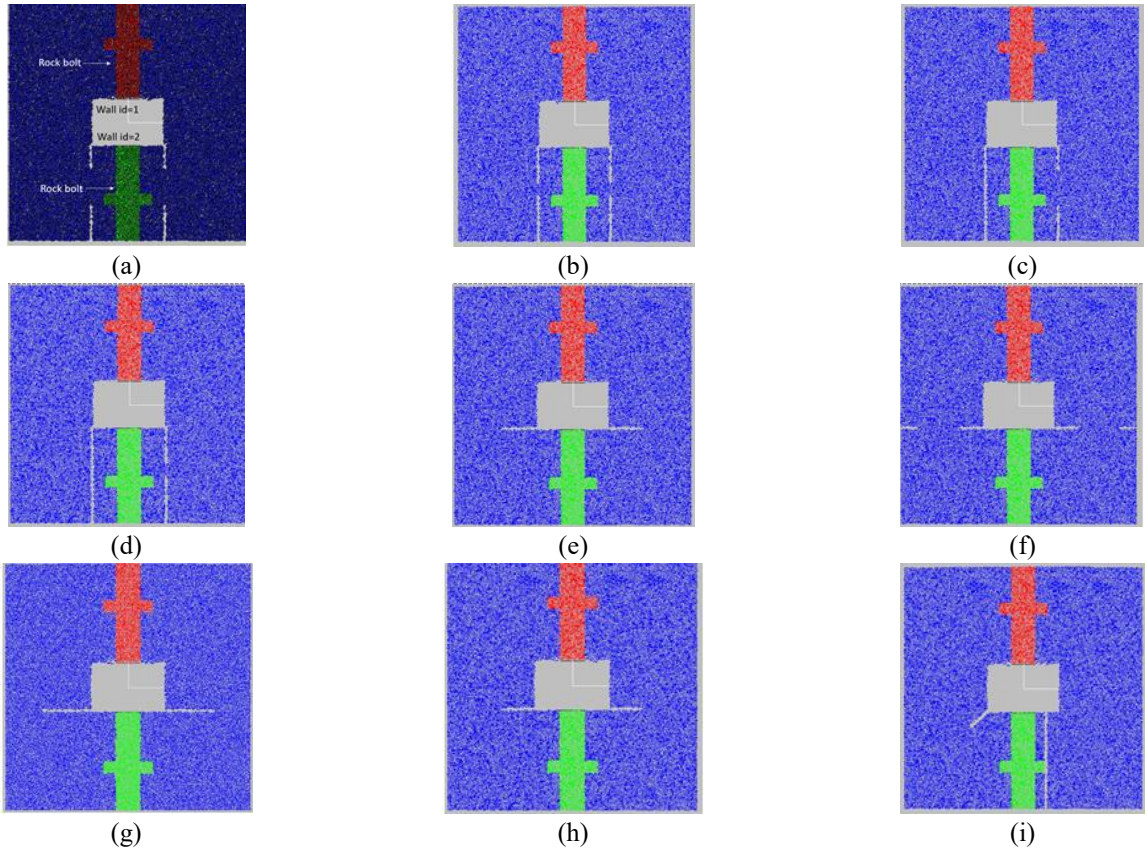

Fig. 8 Numerical models consisting non-persistent joint which have the same configuration with experimental samples

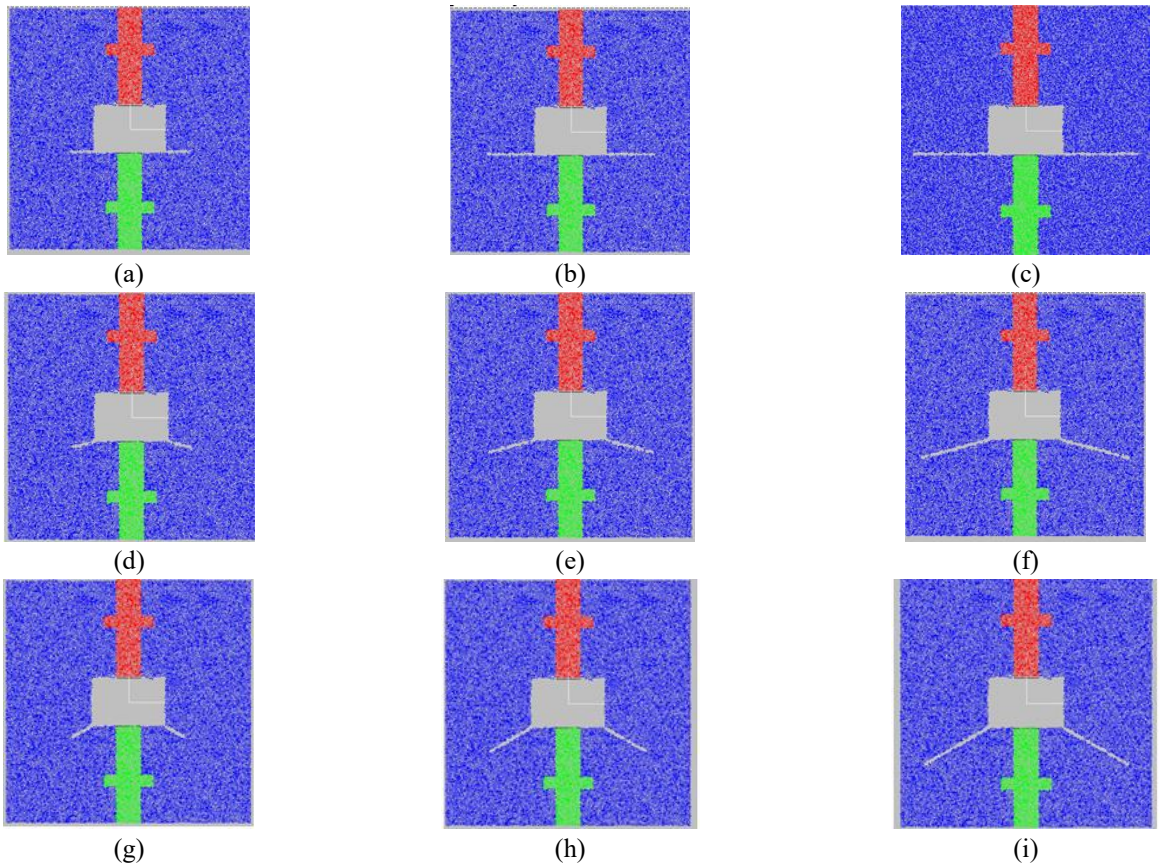

Fig. 9 Numerical models consisting non-persistent joint with angle of 0°, 15°, 30°, 45°, 60°,75°, 90° and length of 1.5 cm, 3 cm and 4.5 cm

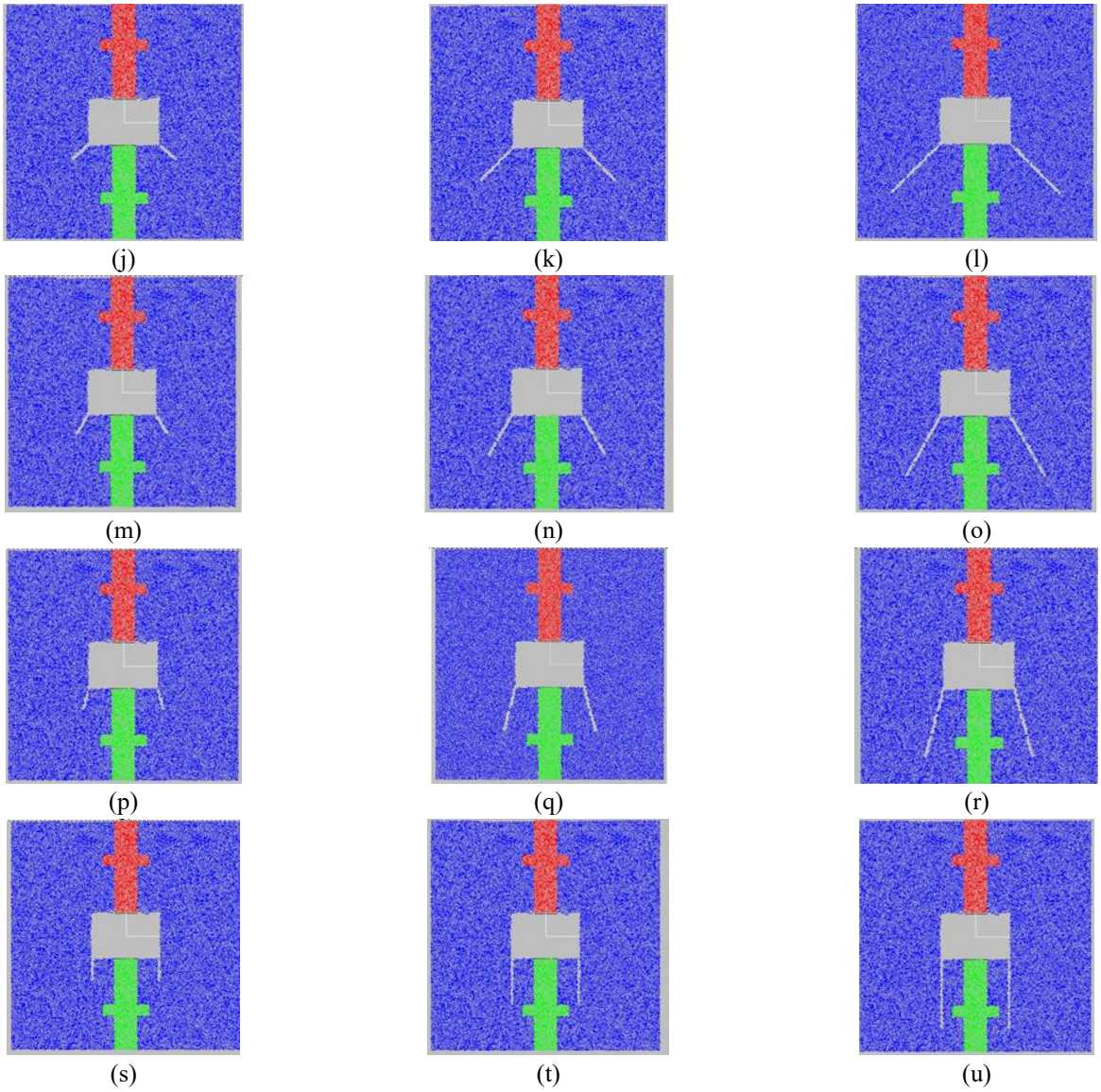

(j) (k) (l)

(m) (n) (o)

(p) (q) (r)

(s) (t) (u)

Fig. 9 Continued

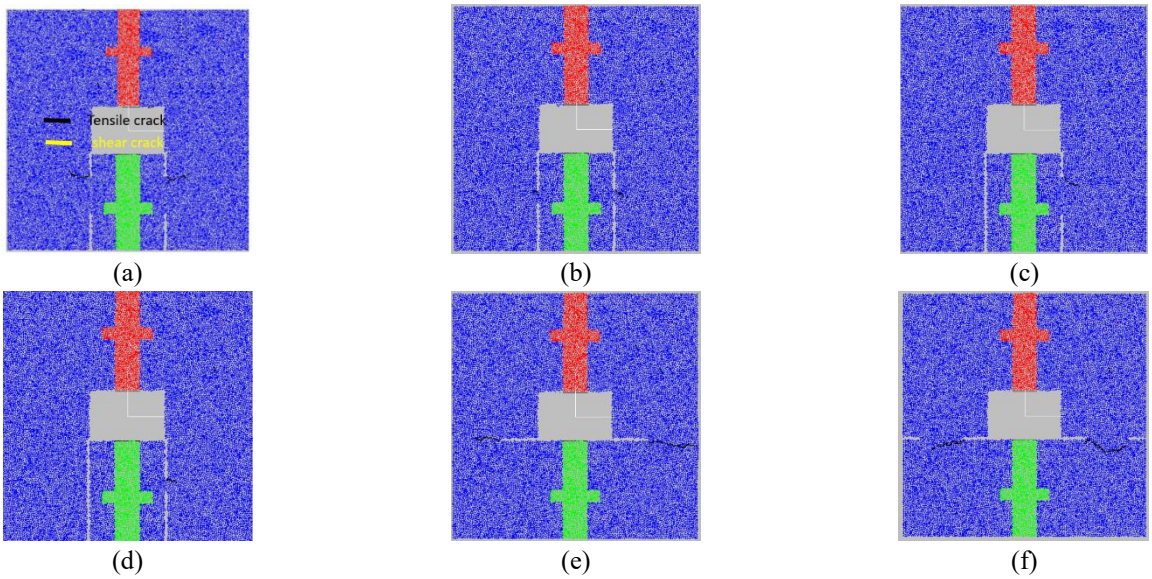

(a) (b) (c)

(d) (e) (f)

Fig. 10 Failure pattern in numerical models containing non-persistent joint under loading rate of 0.01 mm/sec

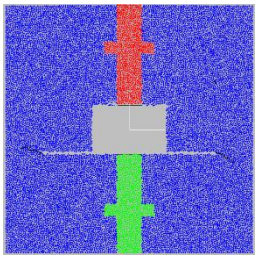
(g)

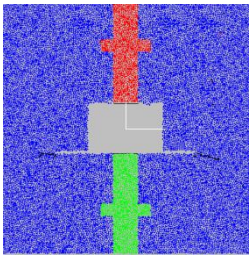
(h)

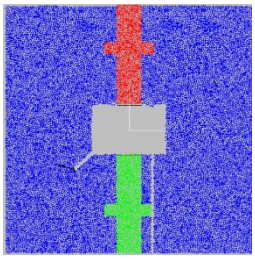
(i)

Fig. 10 Continued

(Potyondy and Cundall 2004, Lin *et al.* 2020a, 2021). The process involves: particle generation, packing the particles, isotropic stress installation (stress initialization), floating particle (floater) elimination and bond installation. Since the specimens were small gravity effect and the gravity-induced stress gradient effect on the macroscopic behavior is neglectable. Direct tensile test was carried out to calibrate the properties of model materials in bonded particle model. For this purpose, a box model was generated in the PFC2D. The PFC sample had the dimensions of 150 mm × 150 mm. An entire number of disks used in making the box sample was 15389 and their minimum radius was 0.27 mm. A rectangular space with dimensions of 30mm* 20mm was removed from center of model so a rectangular pore was generated (Fig 6a). Two rock bolts created in upper and lower of the space. Dimensions of rock bolts are 10 mm * 65mm (Fig 6a). The bolt is represented by a cluster of balls with parallel bonds that meet the requirements of the force-displacement law. Parallel bond transmits both forces and torque between disks, which is consistent with the stress state in a bolt. The micro parameters of the bolt are determined via the bolt pull-out test, as shown in Fig. 7(a). The micro parameters of the bolt are shown in Table 1. Fig. 7(b) describes the stress-strain obtained by pull out test. When the magnitude of the axial stress in the bolt exceeds the maximum normal stress, the bonds will break, and the bolt will lose its bearing capacity. The tensile strength of simulated rock bolt was 360 MPa. It was assumed that the bond failure occurs in rock bolt. Two walls with length of 10 mm were situated on the rock bolts (Fig. 6(a)). Walls id 1 and 2 were moved in positive side of Y direction and in negative side of Y direction, respectively (Fig. 6(a)). The wall velocity was 0.01 mm/sec. Fig. 6(a) and 6(b) shows the experimental and numerical failure patterns. The results showed that there is well matching between the tensile failure of experimental test and numerical simulation. Also, the obtained tensile strength from the numerical models agreed well with the experimental values, as indicated in Table 2. The proposed micro parameters for calibration of intact rock were presented in Table 3.

4.3 Numerical compressive tests on the non-persistent open joint

After calibration of PFC2D, direct tensile tests for jointed model were numerically simulated by creating a box model in the PFC2D (by using the calibrated micro-parameters) (Figs. 8 and 9). The PFC specimen had the dimensions s of 150 mm × 150 mm. A total of 15389 disks with a minimum radius of 0.27 mm were used to make the box specimen. A rectangular space was removed from center of model so a rectangular hole was generated (Figs. 8 and 9). Dimensions of hole was 30 mm*20 mm was. Two rock bolts created in upper and lower of the space. Dimensions of rock bolts are 10 mm * 65mm (Figs. 8 and 9). Two sets of non-persistent joint were prepared. The first sets were similar to experimental one (Fig. 8). In the second sets, two edge joints with lengths of 1.5 cm, 3 cm and 4.5 cm were prepared. The angle of these joint related to horizontal axis were 0, 15, 30, 45, 60, 75, and 90 (Fig. 9). Two walls with length of 10 mm were situated on the rock bolts. Walls id 1 and 2 were moved in positive side of Y direction and in negative side of Y direction, respectively. The walls have two high and low velocity rates of 0.01 mm/sec and 0.0001 mm/sec, respectively. In these velocity rates, it is possible to determine the effect of loading rate on the interaction between rock bolt and non-persistent joints.

4.4 Numerical outputs

a. Failure pattern of numerical models which have the same configurations with experimental samples under loading rate of 0.01 mm/sec

Fig. 10 shows the failure pattern of numerical models which have the same configurations with experimental samples under loading rate of 0.01 mm/sec. the tensile crack and shear crack were depicted by black line and red line, respectively. In all models, tensile cracks were originated at tip of the joint and propagated perpendicular to tensile load direction. By comparison between the Fig. 10 and Fig. 4, it's clear that the failure patterns occur in numerical tests and experimental tests under 0.01 mm/sec of loading rate are almost identical.

b. Failure pattern of numerical models which have the same configurations with experimental samples under loading rate of 0.0001 mm/sec

Fig. 11 shows the failure pattern of numerical models which have the same configurations with experimental samples under loading rate of 0.0001 mm/sec. the tensile crack and shear crack were depicted by black line and red line, respectively. In all models, tensile cracks were originated at tip of the joint and propagated nearly diagonal to the tensile load direction. By comparison between Fig. 11 and Fig. 10, it could be concluded that the crack propagation angle related to tensile load direction was decreased by decreasing the tensile loading rate.

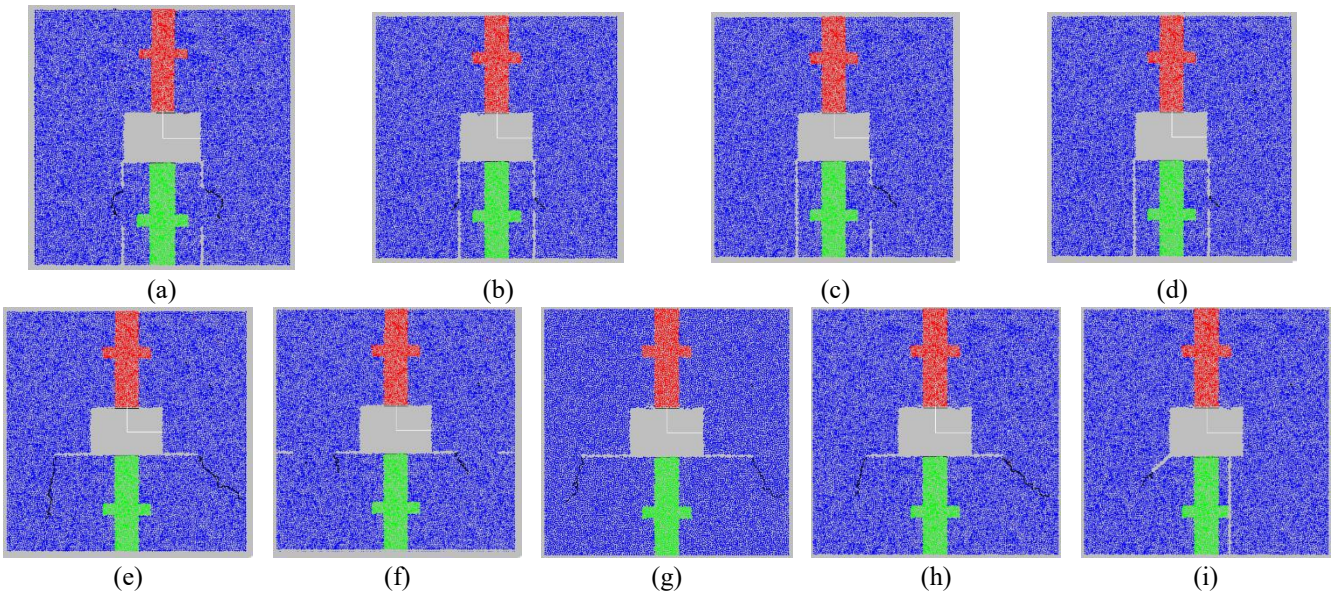

Fig. 11 Failure pattern in numerical models containing non-persistent joint under loading rate of 0.0001 mm/sec

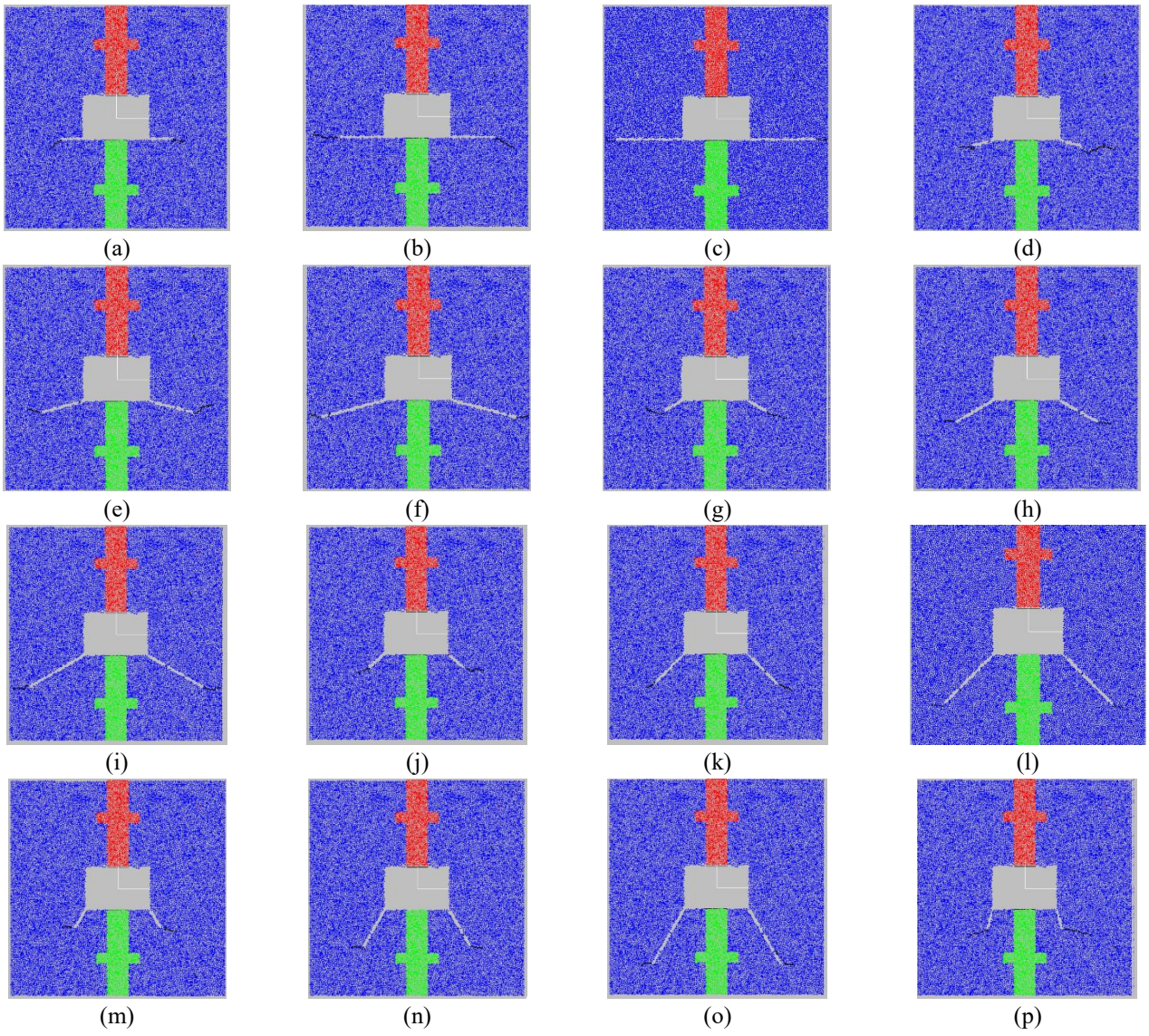

Fig. 12 Failure pattern in numerical models containing non-persistent joint under loading rate of 0.01 mm/sec

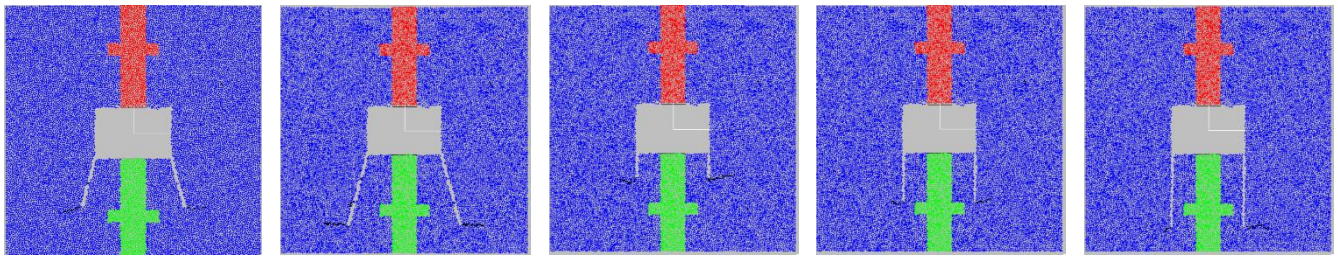

(q) (r) (s) (t) (u)

Fig. 12 Continued

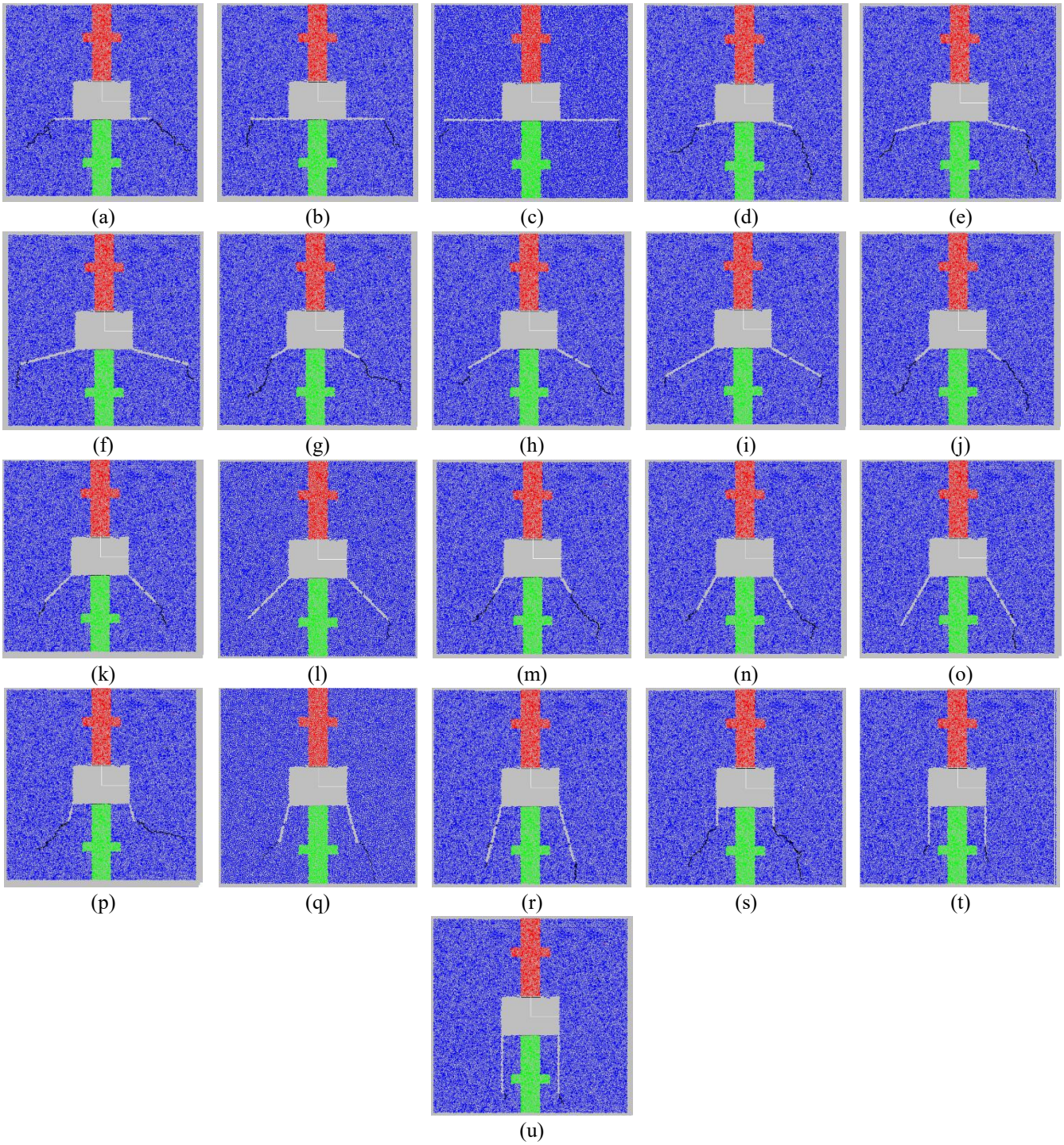

(a) (b) (c) (d) (e)

(f) (g) (h) (i) (j)

(k) (l) (m) (n) (o)

(p) (q) (r) (s) (t)

(u)

Fig. 13 Failure pattern in numerical models containing non-persistent joint under loading rate of 0.0001 mm/sec

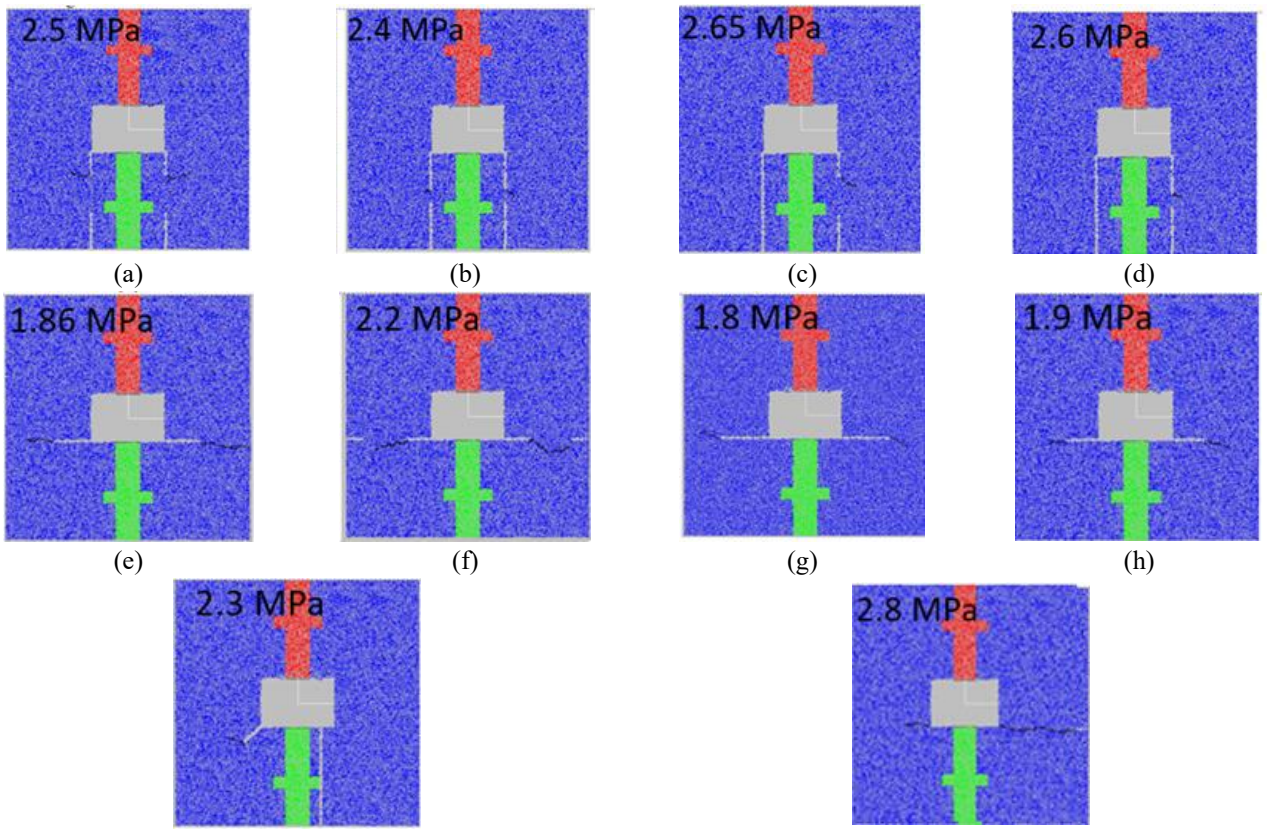

Fig. 14 The effect of crack configuration on the crack origination stress under loading rate of 0.01 mm/sec

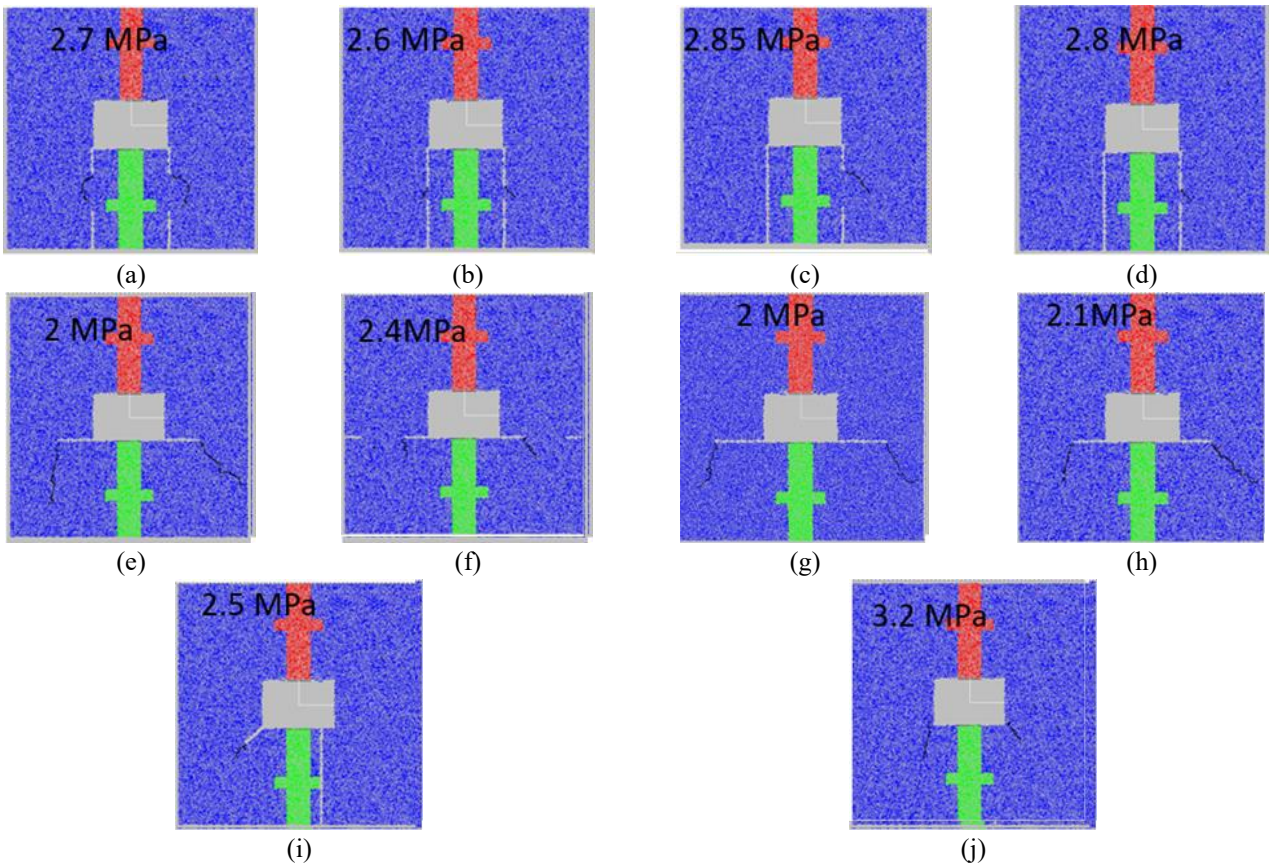

Fig. 15 The effect of crack configuration on the crack origination stress under loading rate of 0.0001 mm/sec

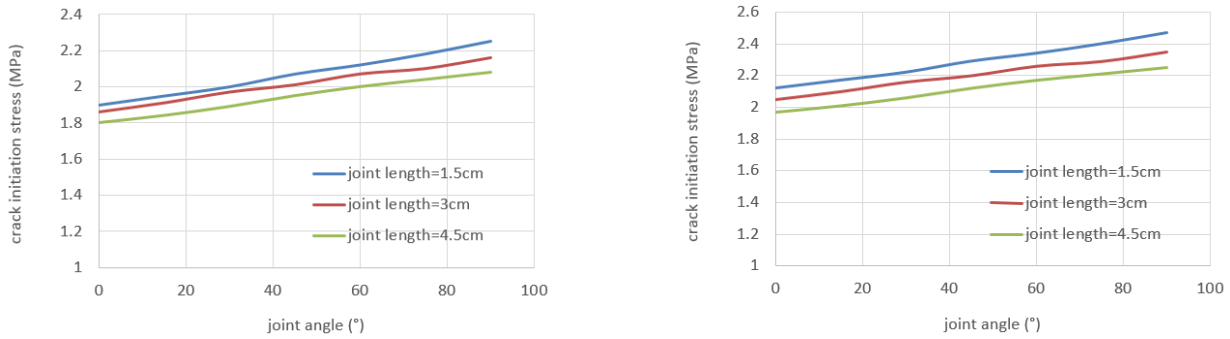

Fig. 16 The effect of joint angle on the crack origination stress for two loading rate of (a) 0.01 mm/sec and (b) 0.0001 m/sec

c. Failure pattern of numerical models with different joint length and different joint angles under loading rate of 0.01 mm/sec

Fig. 12 shows the failure pattern of numerical models with different joint length and different joint angles under loading rate of 0.01 mm/sec. the tensile crack and shear crack were depicted by black line and red line, respectively. In all models, tensile cracks were originated at tip of the joint and propagated perpendicular to tensile load direction. Increasing the joint length and joint angles has not any effect on the crack growth path.

d. Failure pattern of numerical models with different joint length and different joint angles under loading rate of 0.0001 mm/sec

Fig. 13 shows the failure pattern of numerical models with different joint length and different joint angles under loading rate of 0.0001 mm/sec. the tensile crack and shear crack were depicted by black line and red line, respectively. In all models, tensile cracks were originated at tip of the joint and propagated nearly diagonal to the tensile load direction. Increasing the joint length and joint angles has not any effect on the crack growth path. By comparison between fig 1 and fig 2, it could be concluded that the crack propagation angle related to tensile load direction was decreased by decreasing the tensile loading rate.

e. The effect of crack configuration on the tensile crack origination stress

Fig 14 and 15 show the effect of crack configuration on the crack origination stress under loading rates of 0.01 mm/sec and 0.0001 mm/sec, respectively. Also, the crack origination stress in intact model has been depicted in these figures. Totally the following results could be rendered from Figs. 14 and 15.

• The crack origination stress decreases by presence of pre-existing crack within the model.

• Crack origination stress has minimum value whenever the angle of pre-existing crack is 0° (Fig. 14(e), 14(f), 14(g) and 14(h) and Fig 15(e), 15(f), 15(g) and 15(h)).

• The smaller the pre-existing crack length, the smaller the crack origination stress.

• The crack origination stress decreased by increasing the loading rate (by comparison between Figs. 14 and 15).

Fig. 16(a) and 16(b), shows the effect of joint angle on the crack origination stress for two loading rates of 0.01 mm/sec and 0.0001 m/sec, respectively. The results of three joint length have been depicted in this figure. Crack origination stress was increased by increasing the joint angle. The crack origination stress was decreased by increasing the joint length. Also, the crack origination stress decreased by increasing the loading rate.

5. Conclusions

The objective of this paper is to study the effect of loading rates on the interaction between the rock bolts and rock bridges using experimental test and numerical simulation. The results show that:

• Under 0.0001 mm/sec of loading rate, tensile cracks were originated at tip of the joint and propagated nearly diagonal to the tensile load direction.

• Under 0.01 mm/sec of loading rate, tensile cracks were originated at tip of the joint and propagated perpendicular to tensile load direction.

• The crack propagation angle related to tensile load direction was decreased by decreasing the tensile loading rate.

• The tensile failure stress decreases by presence of pre-existing crack within the model.

• Tensile failure force has minimum value whenever the angle of preexisting crack is 0°.

• The smaller the pre-existing crack length, the smaller the tensile failure stress.

• The angle of oriented middle pre-existing notch has not any effect on the tensile failure stress.

• The tensile failure stress is decreased by increasing the number of horizontal preexisting notches.

• The tensile failure stress is decreased by increasing the number of horizontal preexisting notches.

• The crack origination stress decreases by presence of pre-existing crack within the model.

• Crack origination stress has minimum value whenever the angle of preexisting crack is 0°.

• The smaller the pre-existing crack length, the smaller the crack origination stress.

• Crack origination stress was increased by increasing the joint angle.

• The crack origination stress was decreased by increasing the joint length.

• Number of tensile cracks was decreased by increasing

the loading rate.

• The crack growth angle was decreased by increasing the lading rate.

• The same failure pattern occurs in numerical tests and experimental tests under 0.01 mm/sec of loading rate.

References

Barton, N.R. (1986), "Deformation phenomena in jointed rock", *Geotechnique*, **36**(2), 147-167. https://doi.org/10.1680/geot.1986.36.2.147.

Cao, R., Yao, R., Meng, J., Lin, Q., Lin, H. and Li, S. (2020), "Failure mechanism of non-persistent jointed rock-like specimens under uniaxial loading: Laboratory testing", *Int. J. Rock Mech. Min. Sci.*, **132**, 90-104. https://doi.org/10.1016/j.ijrmms.2020.104341.

Das, R., Sirdesai, N.N. and Singh, T.N. (2017), "Analysis of deformational behavior of circular underground opening in soft ground using three-dimensions al physical model", *Proceedings of the 51st US Rock Mechanics/Geomechanics Symposium*, San Francisco, California, U.S.A., June.

Dias, D. (2011), "Convergence-confinement approach for designing tunnel face reinforcement by horizontal bolting", *Tunn. Undergr. Sp. Tech.*, **26**(4), 517-523. https://doi.org/10.1016/j.tust.2011.03.004.

Forbes, B., Vlachopoulos, N., Hyett, A.J. amd Diederichs, M.S. (2017). "A new optical sensing technique for monitoring shear of rock bolts", *Tunn. Undergr. Sp. Tech.*, **66**, 34-46. https://doi.org/10.1016/j.tust.2017.03.007.

Goel, R.K., Swarup, A. and Sheorey, P.R. (2007), "Bolt length requirement in underground openings", *Int. J. Rock Mech. Min. Sci.*, **44**(5), 802-811. https://doi.org/10.1016/j.ijrmms.2006.12.001.

Hu, J., Wen, G., Lin, Q., Cao, P. and Li, S. (2020), "Mechanical properties and crack evolution of double-layer composite rock-like specimens with two parallel fissures under uniaxial compression", *Theor. Appl. Fract. Mech.*, **108**, 101-118. https://doi.org/10.1016/j.tafmec.2020.102610.

Itasca Consulting Group Inc. (2002), Particle Flow Code in 2 Dimensions, Version 30, Itasca Consulting Group Inc., Minneapolis, Minnesota, U.S.A.

Kim H., Kim K., Kim H. and Shin J. (2018) "Anchorage mechanism and pullout resistance of rock bolt in water-bearing rocks", *Geomech. Eng.*, **15**(3), 98-111. http://doi.org/10.12989/gae.2018.15.3.841.

Li, C.C. (2017), "Principles of rock bolting design", *J. Rock Mech. Geotech. Eng.*, **9**(3), 396-414. http://doi.org/10.1016/j.jrmge.2017.04.002.

Li, Z., Soga, K. and Wright, P. (2015), "Behaviour of cast-iron bolted tunnels and their modelling", *Tunn. Undergr. Sp. Tech.*, **50**, 250-269. https://doi.org/10.1016/j.tust.2015.07.015.

Lin, Q., Cao, P., Cao, R., Lin, H. and Meng, J. (2020a), "Mechanical behavior around double circular openings in a jointed rock mass under uniaxial compression", *Arch. Civ. Mech. Eng.*, **20**(1), 33-45. https://doi.org/10.1007/s43452-020-00027-z.

Lin, Q., Cao, P., Mao, S., Ou, C. and Cao, R. (2020b), "Fatigue behaviour and constitutive model of yellow sandstone containing pre-existing surface crack under uniaxial cyclic loading", *Theor. Appl. Fract. Mech.*, **109**, 111-128. https://doi.org/10.1016/j.tafmec.2020.102776.

Lin, Q., Cao, P., Meng, J., Cao, R. and Zhao, Z. (2020c), "Strength and failure characteristics of jointed rock mass with double circular holes under uniaxial compression: Insights from discrete element method modelling", *Theor. Appl. Fract. Mech.*, **109**, 21-38. https://doi.org/10.1016/j.tafmec.2020.102692/

Lin, Q., Cao, P., Wen, G., Meng, J., Cao, R. and Zhao, Z. (2021), "Crack coalescence in rock-like specimens with two dissimilar layers and pre-existing double parallel joints under uniaxial compression", *Int. J. Rock Mech. Min. Sci.*, **139**, 39-53. https://doi.org/10.1016/j.ijrmms.2021.104621.

Luo, X., Cao, P., Lin, Q. and Li, S. (2021), "Mechanical behaviour of fracture-filled rock-like specimens under compression-shear loads: An experimental and numerical study", *Theor. Appl. Fract. Mech.*, **113**, 55-67. http://doi.org/10.1016/j.tafmec.2021.102935.

Palmstrom, A. and Singh, R. (2001), "The deformation modulus of rock masses - Comparisons between in situ tests and indirect estimates", *Tunn. Undergr. Sp. Tech.*, **16**(2), 115-131. https://doi.org/10.1016/S0886-7798(01)00038-4.

Potyondy, D.O. and Cundall, P.A. (2004), "A bonded-particle model for rock", *Int. J. Rock Mech. Min. Sci.*, **41**(8), 1329-1364. https://doi.org/10.1016/j.ijrmms.2004.09.011.

Ramulu, M., Chakraborty, A.K. and Sitharam, T.G. (2009), "Damage assessment of basaltic rock mass due to repeated blasting in a railway tunnelling project - A case study", *Tunn. Undergr. Sp. Tech.*, **24**(2), 208-221. https://doi.org/10.1016/j.tust.2008.08.002.

Saiang, D. and Nordlund, E. (2009), "Numerical analyses of the influence of blast-induced damaged rock around shallow tunnels in brittle rock", *Rock Mech. Rock Eng.*, **42**(3), 421-448. https://doi.org/10.1007/s00603-008-0013-1.

Shen, B. and Barton, N. (1997). "The disturbed zone around tunnels in jointed rock Masses", *Int. J. Rock Mech. Min. Sci.*, **34**(1), 117-125. https://doi.org/10.1016/S1365-1609(97)80037-8

Singh, M., Rao, K.S. and Ramamurthy, T. (2002), "Strength and deformational behaviour of a jointed rock mass", *Rock Mech. Rock Eng.*, **35**(1), 45-64. https://doi.org/10.1007/s006030200008.

Singh, S.P. and Xavier, P. (2005). "Causes, impact and control of overbreak in underground excavations", *Tunn. Undergr. Sp. Tech.*, **20**(1), 63-71. https://doi.org/10.1016/j.tust.2004.05.004.

Wang, H., Li, S., Wang, Q., Wang, D., Li, W., Liu, P., Li, X. and Chen, Y. (2019), "Investigating the supporting effect of rock bolts in varying anchoring methods in a tunnel", *Geomech. Eng.*, **19**(6), 115-123. http://doi.org/10.12989/gae.2019.19.6.485.

Wang, W., Song, Q., Xu, C. and Gong, H. (2018), "Mechanical behaviour of fully grouted GFRP rock bolts under the joint action of pre-tension load and blast dynamic load", *Tunn. Undergr. Sp. Tech.*, **73**, 82-91. https://doi.org/10.1016/j.tust.2017.12.007.

Zhao, T, Zhang, Y., Zhang, Q. and Tan, Y. (2018), "Analysis on the creep response of bolted rock using bolted burgers model", *Geomech. Eng.*, **14**(2), 68-77. http://doi.org/10.12989/gae.2018.14.2.141.

Zou, F., Xia, Z. and Dan, H. (2016), "Theoretical solutions for displacement and stress of a circular opening reinforced by grouted rock bolts", *Geomech. Eng.*, **11**(3), 32-47. http://doi.org/10.12989/gae.2016.11.3.439.

CC